Staufen1 inhibits MyoD translation to actively maintain muscle stem cell quiescence

Antoine de Morrée[a,b,1], Cindy T. J. van Velthoven[a,b,1], Qiang Gan[a,b], Jayesh S. Salvi[a,b], Julian D. D. Klein[a,b], Igor Akimenko[a,b], Marco Quarta[a,b,c], Stefano Biressi[a,b,2], and Thomas A. Rando[a,b,c,3]

[a]Department of Neurology and Neurological Sciences, Stanford University School of Medicine, Stanford, CA 94305; [b]Paul F. Glenn Center for the Biology of Aging, Stanford University School of Medicine, Stanford, CA 94305; and [c]Center for Tissue Regeneration, Repair and Restoration, Veterans Affairs Palo Alto Health Care System, Palo Alto, CA 90304

Edited by Eric N. Olson, University of Texas Southwestern Medical Center, Dallas, TX, and approved September 8, 2017 (received for review May 26, 2017)

Tissue regeneration depends on the timely activation of adult stem cells. In skeletal muscle, the adult stem cells maintain a quiescent state and proliferate upon injury. We show that muscle stem cells (MuSCs) use direct translational repression to maintain the quiescent state. High-resolution single-molecule and single-cell analyses demonstrate that quiescent MuSCs express high levels of Myogenic Differentiation 1 (MyoD) transcript in vivo, whereas MyoD protein is absent. RNA pulldowns and costainings show that MyoD mRNA interacts with Staufen1, a potent regulator of mRNA localization, translation, and stability. Staufen1 prevents MyoD translation through its interaction with the MyoD 3′-UTR. MuSCs from Staufen1 heterozygous (Staufen1$^{+/-}$) mice have increased MyoD protein expression, exit quiescence, and begin proliferating. Conversely, blocking MyoD translation maintains the quiescent phenotype. Collectively, our data show that MuSCs express MyoD mRNA and actively repress its translation to remain quiescent yet primed for activation.

Staufen1 | MyoD | quiescence | satellite cell | muscle stem cell

Adult stem cells exert a key role in the maintenance of organ homeostasis and in the regeneration of damaged tissues (1, 2). The latter property is well illustrated by stem cells residing in skeletal muscle, a tissue with relatively low turnover, but exhibiting a high regenerative potential (3, 4). Adult muscle stem cells (MuSCs) (also called "satellite cells") are absolutely required for productive regeneration to occur as demonstrated by studies in which genetic ablation of MuSCs results in a dramatic impairment in muscle regeneration (5–7).

In undamaged adult muscle, MuSCs exist in a reversible state of prolonged exit from the cell cycle also known as quiescence (8). Upon muscle injury, these cells activate, enter the cell cycle, and expand rapidly to rebuild damaged muscle fibers (9). The control of quiescence is crucial to preserve the regenerative potential of skeletal muscle. Loss of quiescence can result in depletion of the stem cell pool, and this depletion, in turn, negatively affects tissue homeostasis and regenerative potential (10–12). The transition of a quiescent stem cell to an actively proliferating cell is tightly regulated and requires extensive metabolic and transcriptional activity (13, 14).

Recent evidence strongly suggests that stem cell quiescence is an actively maintained state and that activation of cells largely depends on the multiple levels of regulation (10, 11, 15, 16). A recent study showed that the phosphorylation state of the translation initiation factor elF2alpha controls the ability of MuSCs to activate (15). Evidence suggests that MuSCs may be actively poised in a quiescent state to allow for a rapid response to regenerative stimuli to occur (16). Specifically, recent studies showed that Myf5 mRNA is stored in mRNP granules in quiescent MuSCs. During activation, mRNP granules are dissociated, Myf5 mRNA becomes available for translation, Myf5 protein rapidly accumulates, and cells progress along the myogenic program (16).

Similar to Myf5, MyoD is a myogenic determination gene that has been implicated both in the myogenic commitment of muscle progenitors and in the process of MuSC activation. Indeed, the appearance of MyoD protein has been functionally linked with MuSC activation and is controlled at the level of transcription and RNA degradation (17, 18). In this paper, we demonstrate that, contrary to prevailing models, quiescent MuSCs express MyoD transcript in vivo and actively block MyoD translation. When these cells activate, they increase protein translation by relieving this translational block. Therefore, MuSCs exist poised for activation by the regulation of translation of transcripts present in the quiescent state. Furthermore, we discovered that the RNA-binding protein Staufen1 plays a determinant role in this process and consequently in the control of stem cell quiescence.

Results

Quiescent MuSCs Express MyoD Transcript but Not MyoD Protein. It is well established that MyoD protein is undetectable in quiescent, nonactivated MuSCs but increases substantially during the first 24 h of activation, shown perhaps most convincingly by studies of MuSCs associated with single fiber explants (19). Intriguingly, we had previously found that the level of MyoD transcript, as assessed by microarray analysis, was as high in freshly isolated MuSCs from uninjured tissue as in cells isolated 3 days postinjury (20). Indeed, RNA-sequencing (RNA-seq) analysis of MuSCs isolated from uninjured and injured muscle showed comparable MyoD transcript levels (Fig. S1*A*). We also observed MyoD transcript levels, measured by quantitative RT-PCR (qRT-PCR), to be essentially

Significance

This work addresses a fundamental mechanism for the translational control of a master regulator of myogenic differentiation, MyoD, by the RNA binding protein Staufen1. We show that muscle stem cells express the MyoD transcript in the quiescent state in vivo but block its translation through direct repression by Staufen1. Loss of this translational repression leads to MyoD translation and cell cycle entry, highlighting a novel role for MyoD in regulating the exit from quiescence. This mechanism of direct translational repression enables the cells to exist poised for activation and cell cycle entry. These data provide insight in the translational control of muscle stem cell quiescence.

Author contributions: A.d.M., C.T.J.v.V., and T.A.R. designed research; A.d.M., C.T.J.v.V., Q.G., J.S.S., J.D.D.K., I.A., M.Q., and S.B. performed research; A.d.M., C.T.J.v.V., Q.G., J.S.S., J.D.D.K., I.A., M.Q., and S.B. analyzed data; and A.d.M., C.T.J.v.V., and T.A.R. wrote the paper.

The authors declare no conflict of interest.

This article is a PNAS Direct Submission.

Data deposition: The data reported in this paper have been deposited in the Gene Expression Omnibus (GEO) database, https://www.ncbi.nlm.nih.gov/geo (accession no. GSE103603).

[1]A.d.M. and C.T.J.v.V. contributed equally to this work.

[2]Present address: Dulbecco Telethon Institute and Centre for Integrative Biology (CIBIO), University of Trento, 38123 Trento, Italy.

[3]To whom correspondence should be addressed. Email: rando@stanford.edu.

This article contains supporting information online at www.pnas.org/lookup/suppl/doi:10.1073/pnas.1708725114/-/DCSupplemental.

equivalent in freshly isolated MuSCs as in MuSCs cultured for 24 h (Fig. 1*A*), a time when MyoD protein is clearly detectable (Fig. 1 *B* and *C*). Thus, there is clearly a discordance between the levels of MyoD transcript and MyoD protein during this critical transition of MuSCs out of the quiescent state and into the actively proliferating state.

A Majority of Isolated Quiescent MuSCs Express MyoD Transcript. One explanation for the high level of MyoD transcript in the freshly isolated MuSC population, with MyoD protein being undetectable in nearly all cells, would be the presence of rare cells with high levels of transcript. To rule this out, we isolated MuSCs from uninjured muscles and analyzed gene expression by single-cell qRT-PCR. Nearly all cells that were positive for Pax7 transcript were also positive for MyoD transcript (Fig. S1*B*). MuSCs heterogeneously express MyoD (Fig. 1*D*), reflecting approximately a 100-fold difference in expression levels. We also detected heterogeneous, but less variable, levels of MyoD transcript in activated MuSCs isolated 3.5 d after a muscle injury (Fig. 1*E*).

To detect RNA directly, we used single-molecule RNA fluorescence in situ hybridization (smFISH) (21). We found that nearly all MuSCs showed distinct and specific MyoD smFISH quanta (Fig. 1*F* and Fig. S1*C*). On average, MuSCs isolated from uninjured tissue contained 13 MyoD smFISH quanta versus 6 Pax7 smFISH quanta (Fig. 1 *G* and *H*). We detected similar numbers of MyoD smFISH quanta on fiber explants (Fig. S1 *D*

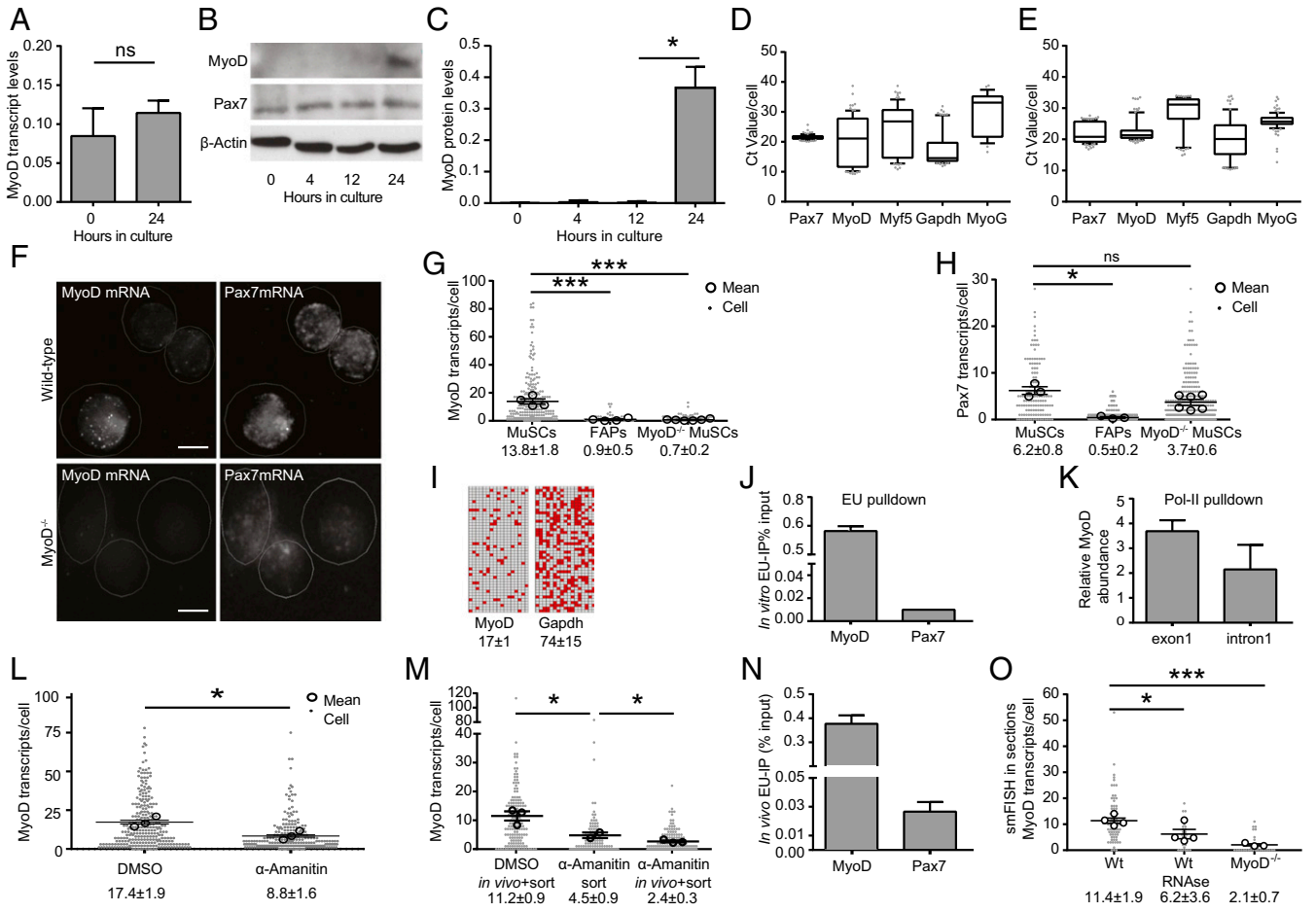

Fig. 1. Active MyoD transcription in MuSCs in vivo. (*A*) qRT-PCR analysis of the MyoD transcript relative to GAPDH in freshly sorted MuSCs and after 24 h in culture. (*B* and *C*) Western blot analysis of MyoD, Pax7, and β-actin protein expression in MuSCs at specified time points after sorting. Representative image (*B*) and quantification of MyoD level corrected for β-actin (*C*). (*D* and *E*) Gene expression of Pax7, MyoD, Myf5, Gapdh, and MyoG was analyzed by qRT-PCR in single cells from uninjured (*D*) or injured (*E*) mice. Raw Ct values are plotted. In *D* the cells with MyoG levels below the limit of detection (57 of 96) were omitted from the graph. (*F*) Freshly isolated MuSCs from wild-type and MyoD$^{-/-}$ mice were fixed and simultaneously hybridized with two differentially labeled probe libraries directed against Pax7 and MyoD and counterstained with DAPI. Single transcripts appear as spots under a fluorescent microscope. "MyoD" and "Pax7" show processed images for those specific channels rendered in grayscale. (Scale bar, 5 μm.) (*G* and *H*) Quantification of smFISH for MyoD (*G*) and Pax7 (*H*) on freshly isolated MuSCs and fibroadipogenic progenitors (FAPs, negative control) isolated from wild-type mice, as well as MuSCs isolated from MyoD$^{-/-}$ mice. Dots denote single cells and circles denote the average per animal. (*I*) Digital PCR chip images with reaction-positive wells shown in red. (*J*) Total and EU-labeled nascent RNA was prepared from MuSCs that were exposed to EU during the isolation procedure. Levels of nascent MyoD and Pax7 transcripts were determined as percentage of total RNA by means of qRT-PCR. (*K*) Association of the active form of RNA polymerase II with the *MyoD1* locus was assessed by ChIP-PCR, using primer pairs that detect exon1 or intron1 of the *MyoD1* gene. Signal was normalized to IgG control. (*L*) RNA transcription during the isolation procedure of MuSCs was inhibited using α-amanitin, and the number of MyoD smFISH quanta per cell was determined. Dots denote single cells and circles denote the average per animal. (*M*) RNA transcription was inhibited in vivo for 4 h and the number of MyoD smFISH quanta was determined in quiescent MuSCs. Dots denote single cells and circles denote the average per animal. (*N*) EU was injected 24 h before isolation of MuSCs from hindlimb muscles and total and EU-labeled nascent RNA was prepared. The levels of nascent MyoD and Pax7 transcripts were determined as percentages of total RNA. (*O*) Quantification of smFISH for MyoD on muscle cryosections from wild-type and MyoD$^{-/-}$ mice, as well as wild-type cryosections pretreated with RNase. Data are reported as mean ± SEM. *$P < 0.05$, ***$P < 0.001$; ns, not significant.

and *E*). The MyoD levels were confirmed using digital PCR, which detected on average 17 MyoD transcripts per cell (Fig. 1*I*).

Two independent assays to measure transcript levels yielded highly comparable results (Fig. S1*B*). We conclude that MuSCs isolated from uninjured skeletal muscle tissue contain, on average, 13–18 molecules of MyoD transcript and that these levels remain relatively constant during MuSC activation, even as the expression levels of MyoD protein increase dramatically.

Isolated Quiescent MuSCs Contain Mature MyoD Messenger RNA. For messenger RNA to be translated, it needs to be fully mature, with a 5′-CAP and a 3′-poly(A) tail. The qRT-PCR analyses made use of intron-spanning primers and suggested that the transcripts are fully spliced and mature (Fig. 1*A*). Immunoprecipitation (IP) of 5′-capped mRNA and IP of 3′-poly(A) mRNA further confirmed the presence of mature MyoD transcripts (Fig. S1 *F* and *G*). Moreover, in vitro translation assays showed that RNA from quiescent MuSCs from wild-type mice, but not from MyoD knockout mice, resulted in detectable MyoD protein (Fig. S1*H*). Together, these results show that the MyoD RNA in freshly isolated quiescent MuSCs is capped, spliced, and polyadenylated and corresponds to mature messenger RNA that can be translated into protein.

Quiescent MuSCs Actively Transcribe MyoD During the Cell Isolation Procedure. As freshly isolated MuSCs are still quiescent but in the earliest stages of activation, we determined whether any of the MyoD transcript detected in freshly isolated cells could have been transcribed during the isolation procedure. Labeling of nascent transcripts with the nucleotide analog 5-ethynyluridine (EU) indeed showed evidence of de novo MyoD transcription during the cell isolation procedure (Fig. 1*J*). Active MyoD transcription in freshly isolated MuSCs was confirmed by chromatin IPs for the active form of RNA polymerase II (serine 5 phosphorylated CTD subunit) showing that it is bound to the MyoD locus (Fig. 1*K*).

To assess the relative amount of MyoD mRNA that was present in vivo before the isolation procedure and any de novo synthesis of MyoD transcript, we isolated MuSCs in the presence of the RNA polymerase II inhibitor α-amanitin (22). As expected, the number of EU-positive cells decreased to ∼20% of that observed without inhibitor (Fig. S1*I*). Approximately 50% of the MyoD transcript detected by smFISH in freshly isolated MuSCs was present in the MuSCs in vivo without any change in the number of cells expressing the transcript (Fig. 1*L*). These data suggest that although active transcription occurs during the cell purification procedure, a substantial proportion of the transcript is already present in the cells in the quiescent state in vivo.

In addition to transcription, RNA degradation might also be occurring during the isolation procedure, leading to an underestimation of the amount of MyoD transcript present in the quiescent MuSCs in vivo. To estimate RNA degradation rates, mice were treated with α-amanitin 4 h before isolation of MuSCs from the diaphragm, a muscle that would be expected to have been exposed to the highest concentrations of the inhibitor. Following continuous treatment with the inhibitor during the isolation procedure, the number of smFISH quanta was ∼25% of that without continuous treatment and ∼50% of that from cells treated with inhibitor only during the isolation procedure (i.e., no treatment in vivo) (Fig. 1*M*). These data suggest a half-life for MyoD transcript of approximately 4 h both in vivo and ex vivo (Fig. S1*J*, see *Methods* for calculations), similar to the MyoD transcript half-life reported in differentiated C2C12 myoblasts (23). This result further supports the conclusion that quiescent MuSCs actively transcribe the *MyoD1* gene in vivo.

Quiescent MuSCs Express MyoD Transcript in Vivo. To directly test for MyoD transcription in vivo, we pulsed mice with a systemic injection of EU and isolated MuSCs after a 24-h chase. Again, we could detect evidence of active MyoD transcription in quiescent MuSCs in vivo (Fig. 1*N*). To definitively determine that most MuSCs in vivo express MyoD messenger RNA, we analyzed muscle cryosections for MyoD smFISH quanta. Because Pax7 antibodies were incompatible with the smFISH protocol, we used a YFP lineage tracer in combination with a Pax7CreER driver to specifically label the MuSCs with YFP (24). Isolated MuSCs of this genetic background express MyoD RNA in an RNA polymerase II-dependent manner, similar to wild-type cells and with a similar half-life (Fig. S1 *K* and *L*). We could detect MyoD smFISH quanta in 90% of YFP-positive cells and found that MuSCs in vivo contain ∼11 MyoD transcripts (Fig. 1*O* and Fig. S1*M*). This shows that MuSCs in vivo contain levels of MyoD RNA that are comparable to those observed in isolated MuSCs, without the confounding synthesis during isolation. In contrast to prevailing models, we conclude that quiescent MuSCs in vivo express MyoD mRNA.

Translational Regulation of the MyoD Transcript. The findings of active MyoD transcription without detectable MyoD protein translation in quiescent MuSCs in vivo, combined with the lack of increased MyoD transcription during ex vivo activation when protein levels increase dramatically, raise the question as to the mechanism of translational repression at play in the quiescent state. Thus, we sought to examine what mechanisms might be active in MuSCs to control the translation of the MyoD transcript. We did not observe any colocalization of MyoD transcript and the RNA granule marker Ddx6 (Fig. S1 *N* and *O*), which prevents Myf5 translation in quiescent MuSCs (16). We therefore looked for other candidate regulators in our transcriptome data (20). We focused on the genes that are most highly expressed in quiescent MuSCs (median expression plus three SDs yielded a list of 2,195 genes). From among these, we selected those that decreased by more than 30% by 36 h after injury, yielding 247 unique gene symbols, including known quiescence genes *Pax7*, *Notch3*, *Hes1*, *CalcR*, and *Spry1*. Gene ontology (GO) analyses revealed that 20 of the 247 gene symbols are annotated as RNA binding proteins and therefore potential candidate repressors of MyoD translation (Fig. S2*A*). Among these 20 candidates, only the RNA binding protein Staufen1, which can control mRNA localization, translation, and degradation (25), has a reported function in myogenic cells (26). Gene expression analysis by qRT-PCR confirmed Staufen1 to be highly expressed in quiescent MuSCs compared with activated MuSCs (Fig. 2*A*). Using C2C12 myoblasts as a model, we observed an enrichment of MyoD transcript after IP of endogenous Staufen1 protein (Fig. 2*B*), confirming that Staufen1 can interact with MyoD mRNA.

Previous reports showed that Staufen1 preferentially binds double-stranded RNA structures in the 3′-UTR of its targets (27, 28). To test whether Staufen1 might also bind to MyoD transcript at its 3′-UTR, we created luciferase reporters for the protein coding sequence or the 3′-UTR of MyoD. IP of Staufen1 from C2C12 cells expressing these reporters showed that Staufen1 interacts with the 3′-UTR–containing reporters but not the reporters containing only the ORF (Fig. S2*B*). Next, we tested whether Staufen1 binds to a secondary structure in the 3′-UTR of MyoD. After treatment of freshly isolated MuSCs with dimethyl sulfate (29), MyoD 3′-UTR amplicons remained detectable, suggesting that they stem from paired, protected nucleotides. In contrast, Pax7 3′-UTR amplicons disappeared from the dimethyl sulfate-treated samples, indicating those are exposed, unpaired nucleotides (Fig. S2*C*). We conclude that Staufen1 protein binds to secondary structures in the MyoD 3′-UTR.

Next, we tested whether Staufen binds to MyoD transcript in MuSCs. Following IP of Staufen1 protein from freshly isolated MuSCs, we indeed could detect enrichment for MyoD transcript (Fig. 2*C*). Interestingly, in addition to the mature, spliced MyoD transcript, we observed intron-retaining MyoD transcripts to co-IP with Staufen1, although the total levels of intron-retaining transcripts were much less than those of mature transcript (Fig. 2*D*).

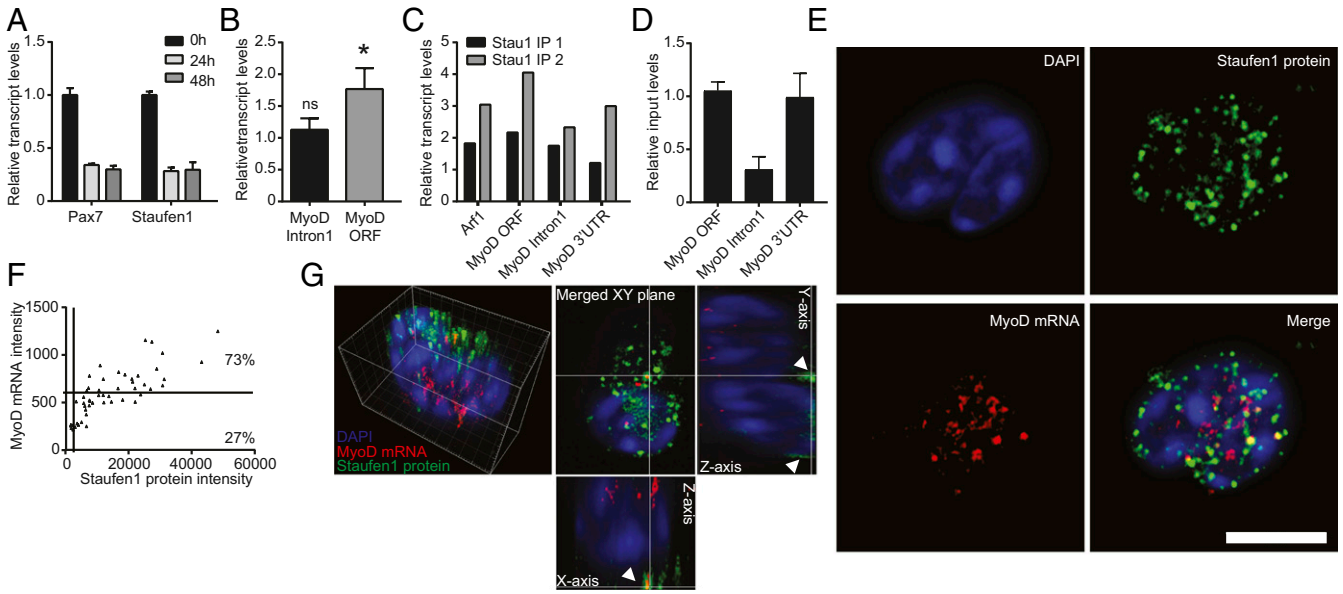

Fig. 2. Localization of MyoD transcript to Staufen1 foci. (*A*) qRT-PCR analysis of the Staufen1 (Stau1) transcript relative to Gapdh in freshly sorted MuSCs and after 24 and 48 h in culture. Pax7 was used as a control. (*B*) RNA-IP using an anti-Staufen1 antibody or IgG control was carried out using C2C12 cells. RNA immunoprecipitates and input lysate RNA were reverse transcribed, amplified using PCR with primer pairs for intron1 or the ORF in MyoD, and plotted relative to IgG control. (*C*) RNA-IP using an anti-Staufen1 antibody was carried out on freshly isolated quiescent MuSCs. RNA immunoprecipitates and input lysate RNA were reverse transcribed and amplified using PCR with primer pairs for intron1, the ORF, or the 3′-UTR in MyoD. Arf1 was used as a positive control. Values were normalized to IgG control and plotted relative to Gapdh. (*D*) qRT-PCR on input material for the Staufen1 IPs with primer pairs for intron1, the ORF, or the 3′-UTR in MyoD. Values are standardized to Gapdh. (*E–G*) Staufen1 protein and MyoD mRNA localization was visualized in quiescent MuSCs by combining smFISH for MyoD (red) with immunofluorescence for Staufen1 (green). Cells were counterstained with DAPI (blue) and imaged by confocal microscopy. (*E*) Representative photographs of colocalization analysis of Staufen1 protein and MyoD1 transcripts. (Scale bar, 5 μm.) (*F*) Quantification of MyoD mRNA smFISH staining at Staufen1 foci. Each triangle represents a Staufen1 focus for which the MyoD and Staufen1 staining intensities are plotted. Solid lines represent thresholds that were determined by staining knockout cells (MyoD) or by using secondary antibodies only (Staufen1). The number of foci above or below the MyoD threshold are given as a percentage. (*G*) A 3D confocal image (*Left*) rendered as a 2D image in the XY plane (*Top Middle*) with orthogonal views of the XZ (*Bottom*) and ZY (*Right*) planes. White lines denote the location of the 2D image in the orthogonal planes. White arrowheads denote the localization of Staufen1 and MyoD mRNA outside the nucleus. Data are reported as mean ± SEM. $*P < 0.05$; ns, not significant.

As a final proof, we costained freshly isolated MuSCs with a Staufen1 antibody and MyoD smFISH probes. We observed a strong correlation between Staufen1 protein immunofluorescence signal and MyoD mRNA staining in the cytosol, with 73% of Staufen1 foci costaining with MyoD transcript, whereas Staufen1 does not colocalize Pax7 mRNA (Fig. 2 *E–G* and Fig. S2 *D* and *E*).

Next we sought to determine whether that interaction between Staufen1 and MyoD results in translational suppression. In vitro translation of MyoD decreased in a dose-dependent manner in response to increasing levels of recombinant Staufen1 protein (Fig. 3 *A–C*). Moreover, coexpression of the luciferase-MyoD reporters described above with Staufen1 in C2C12 myoblasts led to a decrease in luciferase activity for reporters containing the MyoD 3′-UTR, whereas it had no effect on luciferase-MyoD-ORF reporters in C2C12 myoblasts (Fig. 3*D*). We conclude that Staufen1 limits MyoD by suppressing translation and via the interaction of Staufen1 with the 3′-UTR of the MyoD transcript.

We next tested whether Staufen1 can regulate the translation of endogenous MyoD transcripts in quiescent MuSCs. To this end, we overexpressed recombinant GFP-Staufen1 in freshly isolated MuSCs and measured MyoD protein levels after 24 h. In the presence of recombinant Staufen1, MyoD protein levels were significantly reduced (Fig. 3 *E* and *F*). Furthermore, we found that, in control cells, there is a clear positive correlation between the amount of MyoD transcript and the amount of MyoD protein (Fig. S2*F*). Conversely, in GFP-Staufen1 transfected cells, this correlation was lost and higher levels of MyoD transcript did not lead to higher levels of MyoD protein (Fig. 3*G*). These data suggest that Staufen1 can directly limit MyoD translation in quiescent MuSCs.

Next, we analyzed the effect of reduced endogenous Staufen1 protein on MyoD protein levels. As predicted, MuSCs from Staufen1$^{+/-}$ mice had reduced Staufen1 protein levels and higher levels of MyoD protein both in vitro and in vivo (Fig. 3 *H–K* and Fig. S2 *G* and *H*). Because Staufen1 has been reported to control mRNA degradation and translation of the same targets, we tested the effect of Staufen1 on MyoD mRNA levels. Recombinant Staufen1 resulted in a modest reduction in MyoD transcript levels (Fig. S2*I*). Staufen1 itself lacks RNase activity and recruits the RNase Upf1 to degrade transcripts (30). Indeed, we observed Upf1 up-regulation in activating MuSCs and colocalization of MyoD mRNA and Upf1 protein, but not of MyoD mRNA and the Staufen1-independent RNase Upf2 (Fig. S2 *J–N*). Furthermore, knockdown of Upf1 but not Upf2 could rescue the Staufen1-induced reduction in MyoD transcript levels (Fig. S2 *O* and *P*), indicating that Staufen1 can indirectly also control MyoD transcript levels via Upf1. However, MuSCs from Stau1$^{+/-}$ mice express modestly reduced, rather than increased, levels of MyoD mRNA (Fig. S2*Q*). Moreover, in vitro and in vivo transcription inhibition experiments showed that MyoD mRNA turnover occurs at rates comparable to those seen in wild-type cells (Fig. S2 *R* and *S* compare with Fig. 1 *N* and *O*). These data suggest that mRNA degradation plays at most only a minimal role in how Staufen controls MyoD protein levels in the quiescent MuSCs. Indeed, in MuSCs from Stau1$^{+/-}$ mice compared with MuSCs from controls, the MyoD protein level is higher relative to the amount of MyoD transcript per cell (Fig. 3*L*). Conversely, after expression of recombinant Staufen1, the ratio of MyoD protein to MyoD transcript decreased compared with control cells (Fig. S2*T*). We conclude that Staufen1 blocks MyoD translation in quiescent MuSCs.

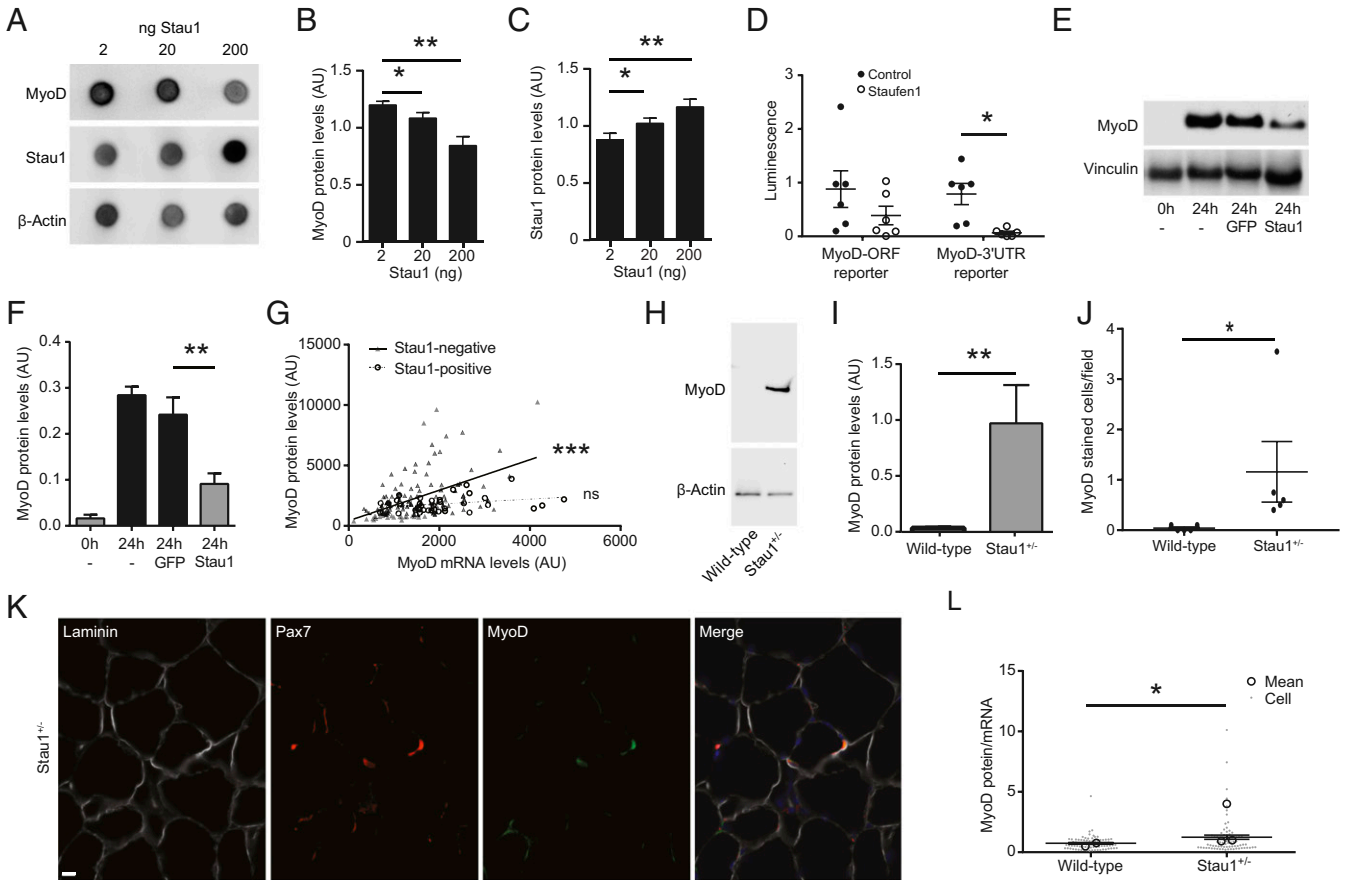

Fig. 3. Staufen1 controls MyoD protein levels in quiescent MuSCs. (*A–C*) Dot blots of in vitro translation assays. MuSC RNA was used as input with increasing amounts of recombinant Staufen1. Shown are representative dot blots (*A*) and quantifications of MyoD (*B*) and Staufen1 (*C*) levels relative to β-actin. (*D*) Luciferase assay in C2C12 cells expressing MyoD Firefly luciferase reporter constructs (Fig. S2*B*) and either GFP or recombinant Staufen1. Transfection levels were controlled using Renilla luciferase. (*E* and *F*) Western blot analysis of MuSCs transfected with Staufen1 for 24 h in vitro. (*E*) Representative Western blot. (*F*) Quantification of MyoD protein levels corrected for Vinculin. (*G*) Quantification of immunofluorescence levels for MyoD protein and smFISH levels for MyoD mRNA after Staufen1 overexpression. Plotted are cells that were Staufen1-positive and Staufen1-negative. Linear regression lines were modeled through the data points to calculate the correlation and statistical significance between mRNA and protein levels. (*H* and *I*) Western blot analysis of Staufen1 protein in MuSCs isolated from wild-type and Staufen1$^{+/-}$ mice. β-Actin was used as a control. Representative image is shown in *H* and quantification of Staufen1 levels relative to β-actin is shown in *I*. (*J*) The number of MyoD-positive cells was scored in cryosections of tibialis anterior (TA) muscles from wild-type and Staufen1$^{+/-}$ mice. (*K*) Representative cryosections from TA muscles from Staufen1$^{+/-}$ mice stained for Laminin (white), Pax7 (red), and MyoD (green). (Scale bar, 10 μm.) (*L*) Quantification of immunofluorescence levels for MyoD protein and smFISH levels for MyoD mRNA in MuSCs freshly isolated from wild-type and Staufen1$^{+/-}$ mice. Plotted is the ratio of protein/mRNA for single cells. Dots denote cells and circles denote the average per animal. Data are reported as mean ± SEM. *$P < 0.05$, **$P < 0.01$, ***$P < 0.001$.

Staufen1 Maintains MuSC Quiescence in Vitro and in Vivo. Having established that Staufen1 can interact with MyoD transcript in quiescent MuSCs and limit its translation, we asked whether this process has any impact on MuSC function in vivo. Analysis of MyoD knockout mice showed that MuSCs without MyoD are slower to divide compared with wild-type cells (31, 32). We therefore asked whether the Staufen1-MyoD axis impacts the propensity of MuSCs to break quiescence and begin proliferating. Nearly twice as many Staufen1$^{+/-}$ MuSCs were 5-ethynyl-deoxyuridine (EdU)-positive after 24 hours in culture compared with wild-type cells (Fig. 4*A*). Similar results were obtained with fiber explants and by knocking down Staufen1 in vitro with siRNAs or by knocking down Staufen1 in vivo with antisense oligonucleotide morpholinos (Fig. 4*B* and Fig. S3 *A–C*). The increased EdU uptake in Staufen1$^{+/-}$ MuSCs could be mitigated by siRNA-induced reduction of MyoD (Fig. 4*A*). We next asked whether Staufen1 similarly regulates MuSC quiescence in vivo. Following 3 days of systemic EdU injections, ~2% of the cells from wild-type animals showed EdU uptake, consistent with these cells being in a quiescent state, whereas, 7% of the cells from Staufen1$^{+/-}$ mice readily incorporate EdU (Fig. 4*C*). A similar increase in EdU incorporation was observed after in vivo knockdown of Staufen1 (Fig. S3*D*). To test whether MyoD levels could impact this effect, we pulsed Staufen1$^{+/-}$:MyoD$^{+/-}$ mice with systemic injections of EdU. Cells isolated from these mice incorporated EdU at levels similar to those of wild-type MuSCs (Fig. 4*C*). These data suggest that loss of Staufen1 increases the propensity of a MuSC to break quiescence and start proliferating, an effect that is dependent upon the presence of MyoD protein. Consistently, the EdU-positive Staufen1$^{+/-}$ MuSCs expressed higher levels of MyoD protein (Fig. S3*E*). To test directly for a causal link between Staufen1 and MyoD in regulating MuSC activation, we coexpressed GFP or GFP-Staufen1 with recombinant MyoD, with or without its 3′-UTR, in MuSCs from MyoD null mice. Strikingly, coexpression of GFP-Staufen1 with the recombinant MyoD without its 3′-UTR had no effect; only when we used a MyoD construct that included the 3′-UTR was Staufen1 able to prevent the increase in EdU incorporation (Fig. 4*D* and Fig. S3 *F* and *G*). To conclusively demonstrate that the Staufen1$^{+/-}$ phenotype depends on MyoD translation, we blocked MyoD translation in vivo using antisense vivo-morpholino oligonucleotides that

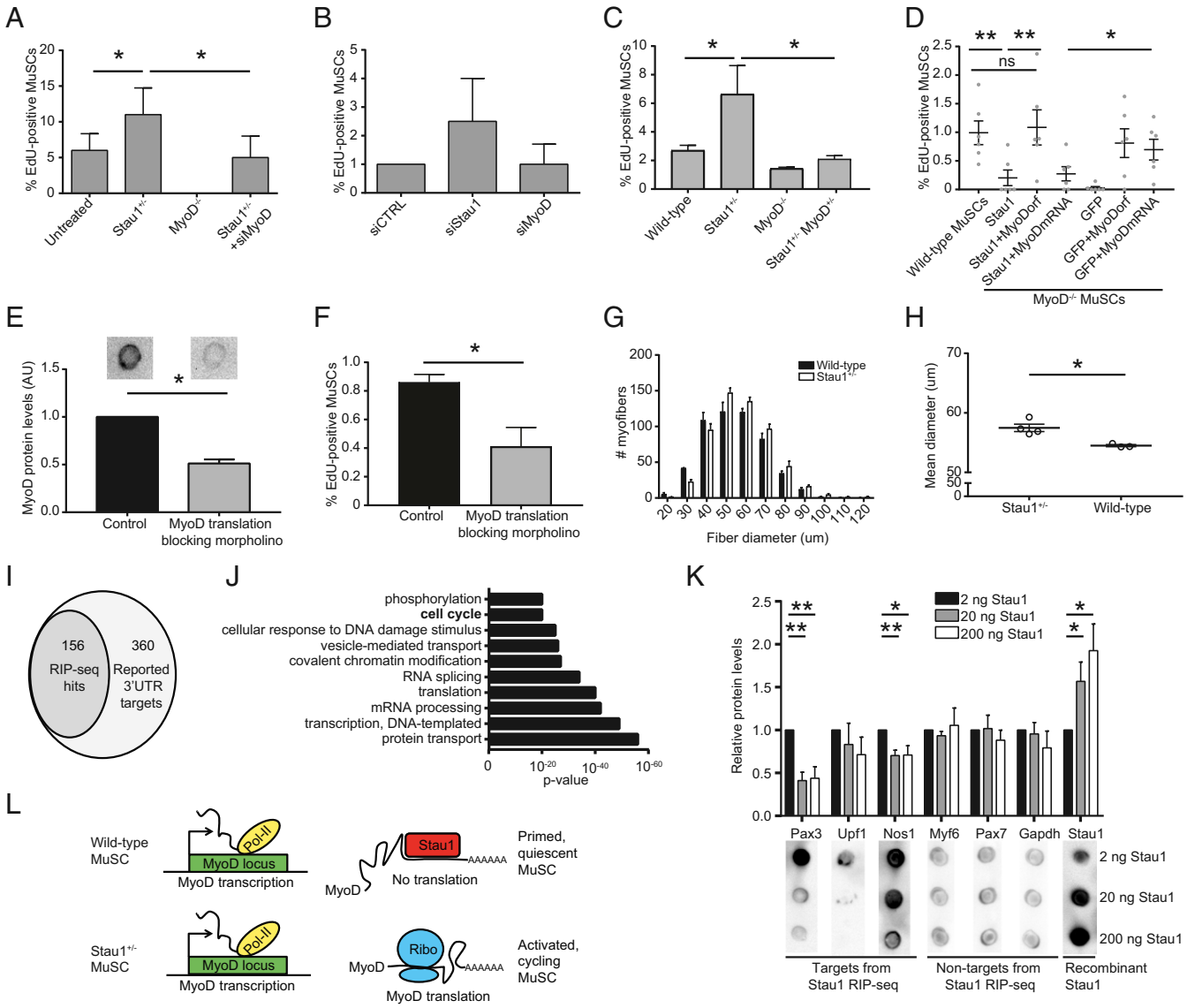

Fig. 4. Staufen1 controls MuSC quiescence in vitro. (*A*) EdU incorporation in MuSCs in vitro after a 24-h pulse. Cells were isolated from wild-type, MyoD$^{-/-}$, and Staufen1$^{+/-}$ mice. The *Rightmost* bar represents Staufen1$^{+/-}$ cells transfected with siRNA against MyoD. (*B*) Wild-type MuSCs were treated with control siRNA, siRNA to MyoD, or siRNA to Staufen1 and pulsed with EdU for 24 h, after which EdU incorporation was measured. (*C*) Wild-type, MyoD$^{-/-}$, Staufen1$^{+/-}$, and Staufen1$^{+/-}$MyoD$^{+/-}$ mice were injected with a dose of EdU every 12 h for 72 h before isolation of MuSCs and quantification of in vivo EdU incorporation. (*D*) MuSCs from MyoD$^{-/-}$ mice were transfected with Staufen1 or GFP expression plasmids, and with plasmids containing either the MyoD ORF ("MyoDorf") or the MyoD ORF plus untranslated regions ("MyoDmRNA"). MuSCs from wild-type mice were used as controls. Cells were pulsed with EdU for 24 h in vitro and EdU incorporation was quantified. (*E*) Control morpholinos or antisense morpholinos complementary to the translation initiation sequence in MyoD were tested in an in vitro translation assay, and MyoD protein was quantified by dot blot. Representative dot blots are depicted *Above* each bar. (*F*) Stau1$^{+/-}$ mice were injected with control morpholinos or antisense vivo-morpholinos to block MyoD translation in vivo and pulsed for 3 d with EdU. Cells were isolated and analyzed for in vivo EdU incorporation. (*G*) Histogram of fiber diameters from cryosections of TA muscles of control and Stau1$^{+/-}$ mice. Sections were stained for laminin and the numbers of myofibers were graphed according to fiber diameter. $P < 0.05$, χ^2 test. (*H*) Quantitative analysis of mean fiber size for uninjured TA muscles in wild-type and Staufen1$^{+/-}$ mice. (*I*) Venn diagram depicting 156 (30%) of 516 reported 3′-UTR–bound Staufen1 targets confirmed by Staufen1 RIP-seq analysis of wild-type MuSCs. (*J*) GO-term analysis of Staufen1 RNA-IP sequencing hits. The top 10 most significantly enriched GO terms are shown. (*K*) Dot blot analysis of in vitro translation assays with MuSC RNA input and increasing concentrations of recombinant Staufen1 protein. Pax3, Upf1, and Nos1 were enriched in Staufen1 RNA-IP sequencing experiments, whereas Myf6, Pax7, and Gapdh were not. Representative dot blots are shown *Below* each set of bars. (*L*) Model of Staufen1-mediated regulation of MyoD. Data are reported as mean ± SEM. *$P < 0.05$, **$P < 0.01$.

blocked MyoD translation in in vitro translation assays (Fig. 4*E*). We injected these vivo-morpholinos, or controls, into Staufen1$^{+/-}$ animals. After blocking MyoD translation in vivo, fewer cells incorporated EdU both in vivo (Fig. 4*F*) and ex vivo (Fig. S3*H*). These results demonstrate that MyoD translation is downstream of Staufen1 in regulating MuSC quiescence in vivo. We conclude that Staufen1 prevents exit of quiescence in vivo by suppressing the accumulation of MyoD protein.

We asked whether the loss of Staufen1-mediated repression of MyoD translation in MuSCs would impact muscle homeostasis and repair. There was a significant increase in fiber diameter in uninjured muscles from Staufen1$^{+/-}$ mice compared with wild-type control mice (Fig. 4 *G* and *H*), demonstrating that a change in MuSC quiescence impacts muscle homeostasis. To assess the effects of Staufen1 deletion on muscle repair, we injured muscles of Staufen1$^{+/-}$ and control mice. Five days after injury, regenerating

myofibers from Staufen1$^{+/-}$ mice were significantly larger than those of control mice (Fig. S3 *I* and *J*). Moreover, this increase was partially reversed in Staufen1$^{+/-}$:MyoD$^{+/-}$ mice. Nevertheless, there was no discernible difference in in vivo EdU incorporation in the proliferating MuSCs, suggesting that Staufen1-MyoD regulation does not alter the proliferative response of activated MuSCs (Fig. S3*K*).

Here we provide evidence for direct translational repression governing the quiescent state of MuSCs and show that the regulation of quiescence is mediated by the translational repression of MyoD. We asked whether the Staufen1-dependent translational repression extends beyond MyoD. Using RNA IP sequencing (RIP-seq), we identified over 3,000 enriched transcripts, including 30% of previously reported 3′-UTR–bound Staufen1 targets (27), in freshly isolated MuSCs (Fig. 4*I*). We performed gene ontology analyses on the Staufen1 target genes and found "cell cycle" among the most enriched categories (Fig. 4*J*), consistent with our findings that Staufen1 controls MuSC quiescence and cell cycle entry. We selected three of the most highly enriched transcripts, Nos1, Pax3, and Upf1, as well as three transcripts that are expressed in quiescent MuSCs but not enriched in the RIP-seq datasets, Myf6, Pax7, and Gapdh. Pax3 was previously shown to be a target of Staufen1 in proliferating C2C12 myoblasts (30). Using in vitro translation assays with quiescent MuSC RNA as input, we show that Staufen1 could repress translation of the three targets, but not the three nontargets, demonstrating that the mechanism of translational repression extends beyond MyoD (Fig. 4*K*).

Discussion

In the current study, our data reveal high levels of MyoD transcripts in quiescent MuSCs in vivo in the absence of any detectable MyoD protein. The resulting pool of transcripts is prevented from being translated into protein by Staufen1, which directly interacts with structures in the MyoD 3′-UTR to suppress translation. MuSCs that lack one Staufen1 allele have increased levels of MyoD protein, break quiescence, and enter the cell cycle more rapidly than wild-type cells. Loss of MyoD prevents cell cycle entry of quiescent Staufen1$^{+/-}$ MuSCs. Accordingly, we propose that Staufen1 limits MyoD translation in quiescent MuSCs to maintain quiescence while priming the cells for rapid activation (Fig. 4*N*).

Prior studies showed that MyoD protein is below the detection level but increases dramatically during MuSC activation (19, 33, 34). Whereas there is general consensus that MyoD protein is undetectable in quiescent MuSCs, contrasting observations have been reported regarding the presence of MyoD transcripts. Initial single-cell studies showed the MyoD transcript to be detectable in a very small number of cells isolated from uninjured tissue and to increase substantially when the cells activate (35, 36). In line with these observations, use of mice in which Cre had been knocked into the MyoD locus (MyoD-iCre) revealed that only 10% of MuSCs on freshly isolated fibers expressed Cre (37). In contrast, transcriptional profiling identified levels of MyoD transcript in freshly isolated MuSCs that were comparable to levels observed in activated MuSCs and therefore difficult to ascribe to a small subpopulation of MyoD-expressing cells (20). Our data reported here clearly show that nearly all MuSCs express MyoD transcript to some extent and, in line with previous reports, do not express the MyoD protein. Importantly, our data revealed a high variability in transcript levels between individual MyoD-expressing MuSCs (Fig. 1*E*), perhaps accounting for divergent findings as to the percentage of quiescent MuSCs expressing the MyoD transcript. Intriguingly, lineage tracing and genetic ablation experiments with the MyoD-iCre mice showed that most MuSCs have transited through a MyoD-positive state during development (37, 38). Although this observation has been attributed to a well-documented expression of MyoD in the developmental precursors of MuSCs, it possibly highlights a dynamic activity of the MyoD locus in the MuSC lineage.

Various posttranscriptional regulatory mechanisms have been shown to be involved in maintaining the quiescent state of MuSCs. Two miRNAs were shown to control transcript fate to maintain quiescence: miR31 sequesters Myf5 into mRNP granules (16) and miR489 suppresses the expression of the oncogene DEK (11). In both cases, suppression of protein expression contributes to maintenance of stem cell quiescence.

Two recent studies found that unchecked MyoD transcription can lead to accumulation of MyoD protein and spontaneous differentiation. In the early stages of activation, Tristetraprolin (TTP), a zinc-finger protein involved in mRNA degradation, targets excess MyoD transcript to mRNA decay pathways to prevent its accumulation (18). Loss of TTP induces a threefold increase in MyoD-positive cells, suggesting that the MuSCs spontaneously activate, possibly due to increased MyoD expression (18). This effect is less pronounced than that observed in Staufen1$^{+/-}$ mice. Our data indicate that control by TTP alone is insufficient, since loss of Staufen1 leads to the accumulation of enough MyoD protein to drive MuSCs to activate and enter the cell cycle. A second study demonstrated that the MyoD locus is repressed by the lysine methyltransferase Suv4-20h1 (17). Knockout of Suv4-20h1 resulted in strong up-regulation of MyoD transcript and protein levels. These cells spontaneously differentiated in noninjured tissue while concurrent genetic ablation of MyoD rescued the phenotype, suggesting that MyoD expression was driving the differentiation. Importantly, we find that MyoD translation is inhibited by Staufen1 and that a loss-of-function allele for Staufen1 causes increased MyoD protein expression in MuSCs, which spontaneously break quiescence. Altogether, these observations suggest that MyoD can drive MuSCs into the cell cycle and trigger their differentiation program. Consistently, MyoD null cells are slower to enter the cell cycle and have a differentiation defect in vitro (31, 32).

Staufen1 is a ubiquitously expressed, double-stranded RNA binding protein that associates with secondary structures. It has been shown to be involved in mRNA transport, splicing, translation, and decay and, as such, plays a key role in the posttranscriptional regulation of gene expression (39–41). Staufen1 regulates terminal differentiation of the human keratinocytes in the epidermis, guides adipogenesis, and plays a role in the early stages of murine embryonic stem cell differentiation (42–44). Only a limited number of studies have investigated the role of Staufen1 in the skeletal muscle, and all of them focused on the control of the differentiation program (26, 30, 45). In multinucleated myotubes, Staufen1 targets several inhibitors of differentiation, including Pax3, for degradation, while in undifferentiated C2C12 myoblasts, it acts as a transcript stabilizer regulating the expression of Dvl2, a repressor of myoblast differentiation (30, 45). Intriguingly, recent experiments with differeniating myoblasts in vitro showed that recombinant Staufen1 reduced MyoD protein expression (26). Although they were unable to identify the molecular mechanism behind this process, these findings are consistent with our data and interpretations.

Our results indicate that Staufen1 regulates the expression of MyoD protein at the translational level in quiescent MuSCs. The fact that quiescent MuSCs have the capacity to regulate MyoD translation through a Staufen1-dependent mechanism points to a cell that is poised to activate. This contrasts with MuSCs at later stages in the myogenic process, which utilize different functions of Staufen1 to regulate the process of terminal differentiation. Previous work showed that Staufen1 controls transcript turnover in proliferating C2C12 myoblasts and that Staufen1 protein levels decrease during differentiation (30). Recent studies using mass cytometry showed MyoD expression to peak early in regeneration after muscle injury and to decrease 6 days after injury (46). It is possible that MyoD expression is tightly regulated and that Staufen1 expression increases when the cells reach the myoblasts stage to control MyoD protein levels. Intriguingly, such a

phasic action has been reported for the Notch signaling pathway, which is similarly involved both in the control of MuSC quiescence and in the modulation of the balance between proliferation and differentiation (10, 12, 47–49). In addition to quiescent MuSCs, other cell types in the chick epiblast have been shown to accumulate MyoD transcripts but not detectable MyoD protein (50). In striking similarity with MuSCs, those cells are also stably committed to the skeletal muscle lineage but are prevented from completing the myogenic program. It is therefore possible that the observations reported here, including the involvement of Staufen1, could also be extended to these cell populations.

In conclusion, we identify the multifunctional protein Staufen1 as a key regulator of MuSC quiescence where it maintains MuSCs in a quiescent, but primed, state by suppressing the translation of MyoD. Our data not only ascribe to Staufen1 a function in the control of stem cell quiescence, but also strongly implicate a role of MyoD protein in the process of MuSC activation out of quiescence.

Methods

Mice. C57BL/6 and ROSA26$^{eYFP/eYFP}$ mice were purchased from The Jackson Laboratory. Pax7$^{CreER/CreER}$ mice were kindly provided by Charles Keller, Oregon Health & Science University (OHSU), Portland, OR. Stau1 null mice (Stau1^{tm1Apa}) were kindly provided by Michael Kiebler, Ludwig Maximilians Universität, Munich. MyoD null mice (MyoD1^{tm1Jea}) were kindly provided by Michael Rudnicki, Ottawa Hospital Research Institute, Ottawa. Animals were crossed with wild-type C57BL/6 animals and maintained as heterozygote breeding pairs to establish littermate controls for the experiments.

Tamoxifen (TMX, Sigma) administration for Cre-recombinase activation in Pax7$^{CreER/+}$:Rosa$^{eYFP/+}$ was performed as previously described (24). TMX was prepared in a mixture of corn oil and 7% ethanol and administered in three doses of 50 mg every 2–3 d by i.p. injection. TMX injections were started in 6- to 8-wk-old mice, and experimental mice were used at 2–4 mo.

Mice were housed and maintained in the Veterinary Medical Unit at Veterans Affairs Palo Alto Health Care Systems. Animal protocols were approved by the Administrative Panel on Laboratory Animal Care of VA Palo Alto Health Care System.

Muscle Regeneration. Muscle regeneration experiments were performed as described previously (51). Briefly, adult mice were anesthetized and injected with 50 μL of 1.5% sterile $BaCl_2$ solution in the tibialis anterior (TA) muscles of each lower hind limb. Five days after the injury, mice were killed. Twelve hours before killing, mice were administered a single dose of EdU via i.p. injection to measure cell proliferation. TA muscles were fixed in 0.5% PFA for 6 h, incubated in 20% sucrose overnight, and flash frozen in Tissue Tek (Sakura) in liquid nitrogen-cooled isopentane. For staining, single cryosections of 7 μm were cut from the midbelly of the muscle using a cryostat. To analyze MuSC proliferation after injury, MuSCs were isolated from injured hind limb muscles by flow cytometry for further analyses.

Flow Cytometry. MuSC isolation was performed as previously described (52). Briefly, hind limb muscles were collected, minced, and digested in Ham's F-10 medium with 10% horse serum (i.e., wash medium) with collagenase II at 500 units/mL at 37 °C for 1.5 h. The muscle suspension was then washed and digested in wash medium with 100 units/mL collagenase II and 2 units/mL dispase for 30 min at 37 °C. Cell suspensions were washed and filtered through a 45-μm cell strainer. MuSCs from Pax7$^{CreER/+}$:Rosa$^{eYFP/+}$ mice were purified by gating mononuclear eYFP-positive cells using a BD-FACS Aria II or BD-FACS Aria III. MuSCs were purified from cell suspensions by negative selection with CD31-FITC, CD45-FITC, and Sca1-Pacific Blue antibodies (BioLegend) and positive selection with VCAM1-biotin and streptavidin-PE-Cy7 antibodies (BioLegend) using a BD-FACS Aria II or BD-FACS Aria III as previously described (52).

RNA Analysis and RT-PCR. To extract total RNA from MuSCs, the RNeasy Plus Micro Kit (Qiagen) was used. Reverse transcription was performed with the High-Capacity cDNA Reverse Transcription Kit (Life Technologies), and qRT-PCR was performed with the LightCycler 480 Probe Master Kit (Roche) in the LightCycler480 II System (Roche). Primer sets used were GapdhFW: tcaagaaggtggtgaagcag and GapdhRV: gttgaagtcgcaggagacaa; Staufen1FW: cggaatttgcctgtgaattt and Staufen1RV: cccctacaaattccccaact; MyoD15′UTRFW: cacgactgctttcttcacca and MyoD15′UTRRV: acaaaggttctgtgggttgg; MyoD1EE2FW: cgacaccgcctactacagtg and MyoD1EE2RV: gctccactatgctggacagg; MyoD13′UTR1FW: acagaacagggaacccagac and MyoD13′UTR1RV: cacctgataaatcgcattgg; MyoD13′UTR2FW: gcgctcttcctttcctcata and MyoD13′UTR2RV: agggctccagaaagtgacaa; Pax7FW: cgagaagaaagccaaacaca and Pax7RV atctgagccctcatccagac; Myf5FW: acagcagctttgacagcatc and Myf5RV: gctggacacggagcttttat; and MyoGFW: agtgaatgcaactcccacag and MyoGRV gcgagcaaatgatctcctg. Relative quantification of transcripts was calculated according to Pfaffl (53).

EU Pulldown. Analysis of nascent MyoD1 transcripts was accomplished by using the Click-iT Nascent RNA Capture Kit (Life Technologies) according to manufacturer's instructions. Briefly, to measure nascent MyoD1 transcripts during isolation of MuSCs, EU was added to every step of the isolation procedure at a concentration of 0.2 mM. Total RNA of 1×10^6 MuSCs was extracted using the RNeasy micro kit according to manufacturer's instructions and mixed with Click-iT reaction mixture (25 μL Click-iT EU buffer, 4 μL 25 mM $CuSO_4$ and 2.5 μL 10 mM biotin azide). Immediately, reaction buffer additive 1 was added, followed by reaction buffer additive 2, exactly 3 min later, and the reaction was carried out for 30 min at room temperature. The RNA was repurified by ammonium acetate precipitation and the purified RNA was bound to 50 μL of streptavidin magnetic beads for 30 min. Beads were then extensively washed and resuspended in a final volume of 25 μL wash buffer 2. The captured RNA was in-bead converted to cDNA as per manufacturer's instructions using the High-Capacity cDNA Reverse Transcription Kit (Life Technologies). To measure nascent transcription in MuSCs in vivo, mice were injected with 1 mg EU dissolved in 100 μL PBS 12 h before isolation of MuSCs. MuSCs were isolated and nascent transcripts were captured as described above.

Immunostaining. Cells were fixed in 3.7% paraformaldehyde for 10 min and permeabilized in 70% ethanol. After a PBS wash, cells were incubated with primary antibodies for 1 h, washed with PBS, and incubated with fluorophore-labeled secondary antibodies for 1 h. Cells were washed and counterstained with 4′,6-diamidino-2-phenylindole (DAPI) and mounted in Vectashield.

Antibodies. Antibodies used in this study are: mouse anti-Pax7 (pax7, DSHB), rabbit anti-GFP (A11122, Life Technologies), chicken anti-GFP (ab15580, Abcam), mouse anti-MyoD (554130, BD Biosciences), rabbit anti-MyoD (13812, Cell Signaling), rabbit anti–β-actin HRP (A3854, Sigma), mouse anti-Vinculin (V9131, Sigma), rabbit anti-Staufen1 (bs-9877R, Bioss), and rabbit anti-RNA polymerase II CTD repeat YSPTSPS (phospho S5) ChIP-grade antibody (ab5131, Abcam).

In Vivo Translation Inhibition. Antisense vivo-morpholinos against the translation start site of either Stau1 (gtccacgggcttatacattggtttt) or MyoD (gcggcgatagaagctccatatccca) were synthesized by GeneTools and dissolved in sterile PBS at 0.5 mM concentration. Animals were injected on day 0 and day 3 with 50 μL vivo-morpholino (~25 nmol or 12.5 mg/kg per injection) and the cells isolated on day 7.

Fiber Culture. Extensor digitorum longus muscles were dissected and digested in Ham's F-10 medium with 500 units/mL Collagenase II (54). The fibers were then triturated, washed extensively, and cultured in Ham's F-10 medium containing 10% horse serum and 0.5% chicken embryo extract. Fibers were cultured in suspension. For Pax7 staining, fibers were fixed in 4% PFA for 5 min, washed in 0.2% Triton X-100, and boiled 30 min in 10 mM citrate buffer (pH 6.0) with 0.5% Tween-20 in a double-boiler setup for antigen retrieval. Slides were cooled for 35 min in buffer, washed, and blocked using blocking solution (0.1% Tween, 0.1% BSA, 0.1% nonfat dry milk, and 2.5% donkey serum in PBS). Primary antibody was incubated overnight at 4 °C, washed, and stained with secondary antibody for 1 h at room temperature and then washed and mounted for imaging.

smFISH: Cells, Sections, and Fibers. Probes for smFISH were ordered from BioSearch. Cells were stained as previously described (21) and according to protocols by BioSearch, with the exception that samples were mounted in 2× saline sodium citrate (SSC) buffer and imaged immediately after staining. For staining of skeletal muscle cryosections, TA muscles were isolated and frozen in liquid nitrogen. Tissues were cut to 7-μm sections and air dried before fixation. Single muscle fibers and sections were fixed in 4% PFA with 0.1% Triton and permeabilized overnight in 70% ethanol at 4 °C. Afterward, samples were equilibrated with wash buffer (10% formamide in 2× SSC buffer) and incubated overnight at 37 °C with probes in hybridization buffer (10% formamide in 2× SSC buffer, 10% dextran sulfate, 0.1% ultra-pure BSA). Samples were washed three times for 1 h with wash buffer, then three times for 1 h with 2× SSC buffer, counterstained for DAPI, and imaged using a cooled CCD camera and 63× objective on a Zeiss Axiovision epifluorescence microscope. For smFISH antibody costains, samples were first stained with the smFISH protocol. Primary antibody was added during the last wash step. Samples were

washed in 2× SSC buffer and treated with secondary antibody together with DAPI counterstain. Samples were mounted in 2× SSC buffer. Images were deconvolved with Volocity software (PerkinElmer) and transcripts quantified with FISH-quant (55). For protein and RNA costains, cells were imaged on a Zeiss LSM880 Airyscan confocal microscope. Images were subsequently processed and deconvoluted using ImageJ.

Single-Cell PCR. Single-cell PCR was performed according to Fluidigm protocols, as previously described (56). Single cells were resorted into PCR mix, preamplified for 20 cycles, and diluted. Diluted preamplified mix was loaded on 96 × 96 chips and analyzed with a BioMark HD.

Digital PCR. Digital PCR was performed as described (57) and according to Fluidigm protocols. Five hundred cells were resorted into PCR mix, preamplified for one cycle, diluted for digital PCR on 12 × 12 chips, and analyzed with a BioMark HD. Calculations were performed with dPCR software (Fluidigm) and using the corrections provided as described (57).

DNA and siRNA Transfection. Reverse transfections with DNA plasmid and siRNA were performed with Lipofectamine 2000 (Invitrogen) according to manufacturer's instructions and transfected cells were analyzed 24 h after plating. For ChIP experiments, cells were transfected with X-tremeGENE HP DNA transfection reagent (Roche) according to the manufacturer's protocols, with the following modifications: for one 10-cm plate, 10 μg plasmid DNA (5 μg reporter and 5 μg Staufen1-GFP) was used with a 2.2:1 ratio of reagent to DNA. Cells were harvested 48 h posttransfection.

Cloning. To create Luciferase-MyoD reporters, MyoD sequences were amplified by phusion polymerase (NEB) and cloned into pMIR-report using SacI and SpeI. Primers were MyoD-3′utrFW: tataACTAGTgagatcgactgcagcagcag and MyoD-3′utrRV: ttaaGAGCTCttgtataaattagcgtctttatttcc; and MyoDorfFW: aaggatACTAGTatggagcttctatcgccgcca and MyoDorfRV: aaggatGAGCTCtcaaagcacctgataaatcgcatt. For ectopic expression, the whole MyoD transcript was amplified and cloned into pcDNA3.1-A using BamHI and EcoRI. Primers were MyoDFW: aaggatGGATCCaggggccaggacgccccaggaca and MyoDRV: aaggatGAATTCaaattagcgtctttatttccaacacct. To create GFP-Staufen1 vector, Staufen1 ORF was amplified and cloned into pEGFP-C1 using XhoI and BamHI. Primers were Stau1FW: aattCTCGAGtgtataagcccgtggaccct and Stau1RV: atatGGATCCtcagcacctcccgcacgctg.

ChIP. Anti-Pol II ChIP experiments were performed according to previous protocols (20) with the following modifications. For each ChIP experiment, about 5×10^6 cells were used, which were resuspended in 300 μL lysis buffer and sonicated with a Covaris S2 ultrasonicator to obtain DNA fragments between ∼200 and 300 bp. Cell lysates were precleared with protein A+G Dynabeads (100-04D, Invitrogen) at 4 °C with agitation for at least 3 h. For each ChIP experiment, 5 μg Pol II antibody or normal rabbit IgG antibody (2729, Cell Signaling) was added into the precleared cell lysate. Following incubation at 4 °C with agitation overnight, cell lysate–antibody complexes were centrifuged (18,407 × *g*) for 10 min at 4 °C and the top 90% supernatant was transferred into a new tube before wash, elution, reverse cross-linking, and purification. Purified ChIP DNAs were quantified using the LightCycler 480 (Roche).

RIP. RNA IP was performed using 4×10^5 MuSCs from wild-type or Staufen$^{-/-}$ mice. Cells were homogenized in 50 mM Tris, pH 7.5, 100 mM KCl, 12 mM $MgCl_2$, 1% Nonidet P-40, 1 mM DTT, 200 units/mL Promega RNasin, 1 mg/mL heparin, and Sigma protease inhibitor mixture. Samples were centrifuged at 10,000 × *g* for 10 min. Staufen1 antibody was added to the supernatant and the mixture was rotated for 4 h at 4 °C, after which Protein G magnetic beads were added and the samples were rotated overnight at 4 °C. The following day, samples were placed in a magnet on ice and the pellets were washed three times for 5 min in high-salt buffer (50 mM Tris, pH 7.5, 300 mM KCl, 12 mM $MgCl_2$, 1% Nonidet P-40, 1 mM DTT) and taken up in 300 μL of Qiagen RLT buffer. Total RNA was prepared using the RNeasy Micro kit (Qiagen) according to manufacturer's instructions and quantified using the Qubit RNA HS assay kit and the Qubit Fluorometer (Molecular Probes). For RIP-PCR, immunoprecipitated RNA samples were converted to cDNA with the High-Capacity cDNA Reverse Transcription Kit (Life Technologies), and qRT-PCR was performed with the LightCycler 480 Probe Master Kit (Roche) in the LightCycler480 II System (Roche). IP samples were analyzed alongside input material and IgG controls. The final results were analyzed by ddCt between the Stau1-IP and IgG-IP samples. Values were then set relative to the nontarget transcript Gapdh.

Samples for RIP-seq were processed as follows: synthesis and amplification of cDNA were done using the SMART-Seq v4 Ultra Low Input RNA Kit for sequencing (634893, Clontech). The cDNA was sheared under the following conditions: 5 min with 10% duty cycle, peak power 175 W and 200 cycles per burst in the frequency-sweeping mode (S220 machine, Covaris). The sheared cDNA was purified with 2.2× AMPure XP SPRI beads (A63880, BeckmanCoulter). RNA-seq libraries were generated using the Ovation Ultralow System (0347, NuGEN). A small aliquot from each RNA sample processed was run on a Bioanalyzer High-Sensitivity DNA chip (Agilent) and used for Qubit quantification. High-throughput sequencing was performed on a Hiseq4000 platform, and the samples were mixed at equal concentrations in a single lane. The sequencing quality of all samples was checked using FastQC (www.bioinformatics.babraham.ac.uk/projects/fastqc/). Sequenced reads were aligned against the mouse reference genome version mm10 (Grcm38) using STAR 2.4.0j (58). The number of reads aligning to genes was counted with featureCounts 1.4.6 tool from the Subread package (59). The quality of the countdata was examined by density distribution plotting. Transcripts with zero or very low expression level were filtered out to minimize interference in downstream analysis. Enriched genes were identified using EdgeR version 3.12 (60). Gene ontology analysis was performed using ReViGo (61) and DAVID (62).

Half-Life Measurements. MuSCs were isolated in the continued presence of α-amanitin at 1 μg/mL. Cells isolated in the presence of the DMSO solvent or the α-amanitin were fixed and analyzed by smFISH. The difference in transcript counts was divided by the time of the isolation procedure to establish the half-life (the time in which half of the molecules have been lost) of MyoD transcripts.

Western Blot. Western blot analysis was performed on whole cell extracts of 1×10^5 MuSCs that were counted, washed, and lysed in sample buffer immediately after FACS purification. Lysates were subjected to SDS/PAGE and transferred to PVDF membrane (Millipore). Membranes were incubated in blocking buffer before overnight incubation with primary antibodies, followed by peroxidase-labeled secondary antibodies, and developed using WesternBright ECL reagents (Advansta). Vinculin or β-actin was used as loading control.

Luciferase Assay. Cells were transfected with luciferase reporter constructs and incubated for 48 h. Cells were lysed and prepared with Promega luciferase kit. Luminescence was calculated as relative value of Firefly and Renilla luciferase.

In Vitro Translation Assay. Analysis of the role of Staufen1 in translation of MyoD1 was performed using the Retic Lysate IVT kit (Ambion) according to manufacturer's instructions. Bacterial expressed recombinant Stau1^{55}Δ2-his$_6$ protein (kindly provided by Luc DesGrosseillers, McGill University, Montreal, Canada) was added to the reactions. The reaction products were separated by SDS/PAGE and treated as described above.

Recombinant Protein Production and Purification. Plasmid for Stau1^{55}Δ2-his$_6$ was transformed into DH5a bacteria. Single colonies were grown overnight in 5-mL cultures and diluted 100× the next morning. When the cell suspension reached OD_{600}, cells were stimulated with 1 mM IPTG for 3 h. Cells were spun down and resuspended in lysis buffer [PBS, protease inhibitor tablet, phenylmethylsulfonyl fluoride (PMSF)] and sonicated with 10-s pulses for 3 min. Debris was spun down and the soluble fraction was incubated with prewashed nickel beads for 1 h at 4 °C. Beads were washed five times and eluted with 100 mM imidazole in PBS. Purity was confirmed by SDS/PAGE and Coomassie Blue staining and concentration was measured using bicinchoninic acid (Pierce) on the Nanodrop 200 Spectrophotometer. Freshly purified protein was used for the assays.

RNA Structure PCR. Dimethyl sulfate is highly reactive with solvent-accessible, unpaired residues but unreactive with bases engaged in Watson–Crick interactions. Nucleotides that are strongly protected or reactive to dimethyl sulfate can be inferred to be base paired or unpaired, respectively (29). Single-stranded RNA is damaged by dimethyl sulfate, preventing primer annealing, and does not show up in the PCR. DMSO was used as a control. RNA from wild-type MuSCs was treated with either dimethyl sulfate of DMSO, transcribed into cDNA, and detected by qRT-PCR with primers pairs detecting the 3′-UTRs of MyoD and Pax7.

Proliferation Assay. MuSCs ($2–5 \times 10^5$ cells per chamber) were cultured on ECM (Sigma)-coated eight-well chamber slides (BD Biosciences) in Ham's F-10 medium with 10% horse serum. EdU was added to cell cultures at a concentration of 10 μM and refreshed every 12 h. Incorporation was detected using the Click-iT EdU Imaging Kit (Life Technologies).

Quantification and Statistical Analysis. Statistical parameters, including sample sizes, the definition of center, and statistical significance are reported in the figures and the figure legends. All experiments were performed using three or more animals. Statistical analyses were done in GraphPad Prism 6 with a Student's *t* test. Histogram comparisons were done with a χ^2 test. Protein–RNA correlations were evaluated with linear regression analyses. Unless otherwise indicated, data are reported as mean ± SEM. Data are considered to be statistically significant when $P < 0.05$. In figures, asterisks denote statistical significance $*P < 0.05$, $**P < 0.01$, $***P < 0.001$.

ACKNOWLEDGMENTS. We thank Dr. M. Rudnicki for providing MyoD1^{tm1Jea} mice, Dr. M. Kiebler for providing Stau1^{tm1Apa} mice, Dr. C. Keller for providing Pax7$^{CreER/CreER}$ mice, Dr. L. DesGroseillers for providing Stau1$^{55}\Delta$2-his$_6$ plasmid, and Dr. Corey Cain and Dr. Lusijah Rott and the Palo Alto Veterans Affairs Flow Cytometry Core for assistance with flow cytometry experiments. This work was supported by funding from the Glenn Foundation for Medical Research, the Muscular Dystrophy Association (MDA313960 to A.d.M.), the Facioscapulohumeral Muscular Dystrophy Society (to A.d.M. and T.A.R.), the NIH (R01 AR062185, R37 AG023806, and P01 AG036695 to T.A.R.), and the Department of Veterans Affairs (Biomedical Laboratory R&D Merit Review to T.A.R.).

1. Simons BD, Clevers H (2011) Strategies for homeostatic stem cell self-renewal in adult tissues. *Cell* 145:851–862.
2. Tetteh PW, Farin HF, Clevers H (2015) Plasticity within stem cell hierarchies in mammalian epithelia. *Trends Cell Biol* 25:100–108.
3. Brack AS, Rando TA (2012) Tissue-specific stem cells: Lessons from the skeletal muscle satellite cell. *Cell Stem Cell* 10:504–514.
4. Chang NC, Rudnicki MA (2014) Satellite cells: The architects of skeletal muscle. *Curr Top Dev Biol* 107:161–181.
5. Lepper C, Partridge TA, Fan CM (2011) An absolute requirement for Pax7-positive satellite cells in acute injury-induced skeletal muscle regeneration. *Development* 138:3639–3646.
6. Murphy MM, Lawson JA, Mathew SJ, Hutcheson DA, Kardon G (2011) Satellite cells, connective tissue fibroblasts and their interactions are crucial for muscle regeneration. *Development* 138:3625–3637.
7. Sambasivan R, et al. (2011) Pax7-expressing satellite cells are indispensable for adult skeletal muscle regeneration. *Development* 138:3647–3656.
8. Cheung TH, Rando TA (2013) Molecular regulation of stem cell quiescence. *Nat Rev Mol Cell Biol* 14:329–340.
9. Yin H, Price F, Rudnicki MA (2013) Satellite cells and the muscle stem cell niche. *Physiol Rev* 93:23–67.
10. Bjornson CR, et al. (2012) Notch signaling is necessary to maintain quiescence in adult muscle stem cells. *Stem Cells* 30:232–242.
11. Cheung TH, et al. (2012) Maintenance of muscle stem-cell quiescence by microRNA-489. *Nature* 482:524–528.
12. Mourikis P, et al. (2012) A critical requirement for notch signaling in maintenance of the quiescent skeletal muscle stem cell state. *Stem Cells* 30:243–252.
13. Rodgers JT, et al. (2014) mTORC1 controls the adaptive transition of quiescent stem cells from G0 to G(Alert). *Nature* 510:393–396.
14. Montarras D, L'honoré A, Buckingham M (2013) Lying low but ready for action: The quiescent muscle satellite cell. *FEBS J* 280:4036–4050.
15. Zismanov V, et al. (2016) Phosphorylation of eIF2alpha is a translational control mechanism regulating muscle stem cell quiescence and self-renewal. *Cell Stem Cell* 18:79–90.
16. Crist CG, Montarras D, Buckingham M (2012) Muscle satellite cells are primed for myogenesis but maintain quiescence with sequestration of Myf5 mRNA targeted by microRNA-31 in mRNP granules. *Cell Stem Cell* 11:118–126.
17. Boonsanay V, et al. (2016) Regulation of skeletal muscle stem cell quiescence by Suv4-20h1-dependent facultative heterochromatin formation. *Cell Stem Cell* 18:229–242.
18. Hausburg MA, et al. (2015) Post-transcriptional regulation of satellite cell quiescence by TTP-mediated mRNA decay. *Elife* 4:e03390.
19. Zammit PS, et al. (2002) Kinetics of myoblast proliferation show that resident satellite cells are competent to fully regenerate skeletal muscle fibers. *Exp Cell Res* 281:39–49.
20. Liu L, et al. (2013) Chromatin modifications as determinants of muscle stem cell quiescence and chronological aging. *Cell Rep* 4:189–204.
21. Raj A, van den Bogaard P, Rifkin SA, van Oudenaarden A, Tyagi S (2008) Imaging individual mRNA molecules using multiple singly labeled probes. *Nat Methods* 5: 877–879.
22. Lindell TJ, Weinberg F, Morris PW, Roeder RG, Rutter WJ (1970) Specific inhibition of nuclear RNA polymerase II by alpha-amanitin. *Science* 170:447–449.
23. Figueroa A, et al. (2003) Role of HuR in skeletal myogenesis through coordinate regulation of muscle differentiation genes. *Mol Cell Biol* 23:4991–5004.
24. Biressi S, Miyabara EH, Gopinath SD, Carlig PM, Rando TA (2014) A Wnt-TGFβ2 axis induces a fibrogenic program in muscle stem cells from dystrophic mice. *Sci Transl Med* 6:267ra176.
25. Heraud-Farlow JE, Kiebler MA (2014) The multifunctional Staufen proteins: Conserved roles from neurogenesis to synaptic plasticity. *Trends Neurosci* 37:470–479.
26. Ravel-Chapuis A, et al. (2014) The RNA-binding protein Staufen1 impairs myogenic differentiation via a c-myc-dependent mechanism. *Mol Biol Cell* 25:3765–3778.
27. Ricci EP, et al. (2014) Staufen1 senses overall transcript secondary structure to regulate translation. *Nat Struct Mol Biol* 21:26–35.
28. Sugimoto Y, et al. (2015) hiCLIP reveals the in vivo atlas of mRNA secondary structures recognized by Staufen 1. *Nature* 519:491–494.
29. Rouskin S, Zubradt M, Washietl S, Kellis M, Weissman JS (2014) Genome-wide probing of RNA structure reveals active unfolding of mRNA structures in vivo. *Nature* 505: 701–705.
30. Gong C, Kim YK, Woeller CF, Tang Y, Maquat LE (2009) SMD and NMD are competitive pathways that contribute to myogenesis: Effects on PAX3 and myogenin mRNAs. *Genes Dev* 23:54–66.
31. Megeney LA, Kablar B, Garrett K, Anderson JE, Rudnicki MA (1996) MyoD is required for myogenic stem cell function in adult skeletal muscle. *Genes Dev* 10:1173–1183.
32. Yablonka-Reuveni Z, et al. (1999) The transition from proliferation to differentiation is delayed in satellite cells from mice lacking MyoD. *Dev Biol* 210:440–455.
33. Füchtbauer EM, Westphal H (1992) MyoD and myogenin are coexpressed in regenerating skeletal muscle of the mouse. *Dev Dyn* 193:34–39.
34. Yablonka-Reuveni Z, Rivera AJ (1994) Temporal expression of regulatory and structural muscle proteins during myogenesis of satellite cells on isolated adult rat fibers. *Dev Biol* 164:588–603.
35. Grounds MD, Garrett KL, Lai MC, Wright WE, Beilharz MW (1992) Identification of skeletal muscle precursor cells in vivo by use of MyoD1 and myogenin probes. *Cell Tissue Res* 267:99–104.
36. Cornelison DD, Wold BJ (1997) Single-cell analysis of regulatory gene expression in quiescent and activated mouse skeletal muscle satellite cells. *Dev Biol* 191:270–283.
37. Kanisicak O, Mendez JJ, Yamamoto S, Yamamoto M, Goldhamer DJ (2009) Progenitors of skeletal muscle satellite cells express the muscle determination gene, MyoD. *Dev Biol* 332:131–141.
38. Wood WM, Etemad S, Yamamoto M, Goldhamer DJ (2013) MyoD-expressing progenitors are essential for skeletal myogenesis and satellite cell development. *Dev Biol* 384:114–127.
39. Dugré-Brisson S, et al. (2005) Interaction of Staufen1 with the 5′ end of mRNA facilitates translation of these RNAs. *Nucleic Acids Res* 33:4797–4812.
40. Kiebler MA, et al. (1999) The mammalian staufen protein localizes to the somatodendritic domain of cultured hippocampal neurons: Implications for its involvement in mRNA transport. *J Neurosci* 19:288–297.
41. Kim YK, Furic L, Desgroseillers L, Maquat LE (2005) Mammalian Staufen1 recruits Upf1 to specific mRNA 3′UTRs so as to elicit mRNA decay. *Cell* 120:195–208.
42. Cho H, et al. (2012) Staufen1-mediated mRNA decay functions in adipogenesis. *Mol Cell* 46:495–506.
43. Gautrey H, McConnell J, Lako M, Hall J, Hesketh J (2008) Staufen1 is expressed in preimplantation mouse embryos and is required for embryonic stem cell differentiation. *Biochim Biophys Acta* 1783:1935–1942.
44. Kretz M, et al. (2013) Control of somatic tissue differentiation by the long non-coding RNA TINCR. *Nature* 493:231–235.
45. Yamaguchi Y, Naiki T, Irie K (2012) Stau1 regulates Dvl2 expression during myoblast differentiation. *Biochem Biophys Res Commun* 417:427–432.
46. Porpiglia E, et al. (2017) High-resolution myogenic lineage mapping by single-cell mass cytometry. *Nat Cell Biol* 19:558–567.
47. Conboy IM, Rando TA (2002) The regulation of notch signaling controls satellite cell activation and cell fate determination in postnatal myogenesis. *Dev Cell* 3:397–409.
48. Shawber C, et al. (1996) Notch signaling inhibits muscle cell differentiation through a CBF1-independent pathway. *Development* 122:3765–3773.
49. Nofziger D, Miyamoto A, Lyons KM, Weinmaster G (1999) Notch signaling imposes two distinct blocks in the differentiation of C2C12 myoblasts. *Development* 126:1689–1702.
50. Gerhart J, et al. (2007) Cells that express MyoD mRNA in the epiblast are stably committed to the skeletal muscle lineage. *J Cell Biol* 178:649–660.
51. Luo D, et al. (2017) Deltex2 represses MyoD expression and inhibits myogenic differentiation by acting as a negative regulator of Jmjd1c. *Proc Natl Acad Sci USA* 114: E3071–E3080.
52. Liu L, Cheung TH, Charville GW, Rando TA (2015) Isolation of skeletal muscle stem cells by fluorescence-activated cell sorting. *Nat Protoc* 10:1612–1624.
53. Pfaffl MW (2001) A new mathematical model for relative quantification in real-time RT-PCR. *Nucleic Acids Res* 29:e45.
54. Rosenblatt JD, Lunt AI, Parry DJ, Partridge TA (1995) Culturing satellite cells from living single muscle fiber explants. *In Vitro Cell Dev Biol Anim* 31:773–779.
55. Mueller F, et al. (2013) FISH-quant: Automatic counting of transcripts in 3D FISH images. *Nat Methods* 10:277–278.
56. Quarta M, et al. (2016) An artificial niche preserves the quiescence of muscle stem cells and enhances their therapeutic efficacy. *Nat Biotechnol* 34:752–759.
57. Sanders R, Mason DJ, Foy CA, Huggett JF (2013) Evaluation of digital PCR for absolute RNA quantification. *PLoS One* 8:e75296.
58. Dobin A, et al. (2013) STAR: Ultrafast universal RNA-seq aligner. *Bioinformatics* 29: 15–21.
59. Liao Y, Smyth GK, Shi W (2014) featureCounts: An efficient general purpose program for assigning sequence reads to genomic features. *Bioinformatics* 30:923–930.
60. Robinson MD, McCarthy DJ, Smyth GK (2010) edgeR: A Bioconductor package for differential expression analysis of digital gene expression data. *Bioinformatics* 26: 139–140.
61. Supek F, Bošnjak M, Škunca N, Šmuc T (2011) REVIGO summarizes and visualizes long lists of gene ontology terms. *PLoS One* 6:e21800.
62. Huang da W, et al. (2009) Extracting biological meaning from large gene lists with DAVID. *Current Protocols in Bioinformatics* (John Wiley & Sons, Ltd., Hoboken, NJ), Chap 13, Unit 13.11.